

Corrosion Behavior of Drill Pipe Steel in CO₂-H₂S Environment

Yisheng Hu^{1*}, Ping Guo¹, Zhiwu Yao², Zhouhua Wang¹, Olujide Sanni³

¹ State Key Laboratory of Oil and Gas Reservoir Geology and Exploitation, Southwest Petroleum University, Chengdu, 610500, China

² Sichuan Geophysical Company, CNPC, Chengdu, 610213, China

³ School of Mechanical Engineering, University of Leeds, Leeds, LS2 9JT, UK

*E-mail: huyisheng008@yahoo.com

Received: 19 April 2017 / Accepted: 17 May 2017 / Published: 12 June 2017

In this paper, scanning electron microscopy, potentiodynamic polarization tests and electrochemical impedance spectroscopy were used to examine the effect of H₂S concentration on H₂S/CO₂ corrosion of pipeline steel. The results showed that the corrosion process of the steel when H₂S coexists with CO₂ at different H₂S concentrations is related to the morphology and consistency of the corrosion product film. When a small quantity of H₂S was added, the surface area of the anode reaction zone decreased due to the continuous adsorption and separation of more substantial FeS deposits or a greater amount of FeHS⁺ ions on the steel surface. At the same time, the dual layer capacitance decreased, while the anion adsorption capacity improved. Consequently, the inhibition of the corrosion process was realized. After the addition of a small quantity of H₂S under the environment such that H₂S coexists with CO₂, the general corrosion rate of the steel declined quickly. Some elements of the corrosion product film became loose or even diminished when H₂S concentration became higher. As a result, the protective effect of the corrosion product film was reduced, and the rate of corrosion increased.

Keywords: H₂S; Corrosion; Electrochemical impedance spectroscopy; Carbon dioxide

1. INTRODUCTION

The inner corrosion of pipe steel when CO₂ coexists with H₂S is a critical issue for both upstream and downstream oil and gas equipment [1-5]. The corrosive environment in the presence of both CO₂ and H₂S results in severe damage to tubes, pipelines, as well as system facilities. While the issues relevant to CO₂/H₂S corrosion of tubing steel have been studied for more than 60 years since the first studies in 1940, the literature on this subject is still perplexing and sometimes ambivalent [6]. Particularly, with the constant rise in energy demand, operational activities must be performed in

severe environments with high H₂S and CO₂ concentrations, such as in the Chinese Sichuan and Changqing oil fields. Therefore, understanding, prediction and manipulation of corrosion under this kind of environment are a critical challenge for effective equipment design and management, and the consequent guaranteed integrity.

The existing reports have proved that the impact of H₂S on the corrosion of CO₂ changes with different H₂S concentrations [7-9]. It is found that low levels of H₂S have several effects on CO₂ corrosion. H₂S not only serves as an accelerant of anodic dissolution through sulfide adsorption and the change of the pH to accelerate the corrosion but can also reduce the rate of CO₂ corrosion through the development of a protective sulfide coating [10, 11]. Additionally, H₂S affects the category and attributes of the developed corrosion coatings, either enhancing or damaging them [12]. Pots *et al.* stated that for P/P >500, the corrosion process was controlled by CO₂ corrosion, but for P/P <20, it was the H₂S corrosion that played the main role within this mechanism, and for the intermediate 20 < P/P < 500 range, the process was controlled by both factors. [13]. It should be emphasized that the majority of these studies were carried out in the low H₂S/CO₂ content environment, so that the studies of the corrosion process in the high H₂S/CO₂ content environment are currently very limited. Ma *et al.* [14] found that H₂S provides great inhibition under the following environment: a low H₂S concentration, a pH value of 3-5, and a longer immersion period (≥ 2 h). Abelev *et al.* [15] observed that 5 ppm of H₂S inhibits corrosion in the environment that also contain CO₂. Nevertheless, the H₂S/CO₂ corrosion process of steel is related to the development of a sulfide film on the steel surface; this film can assume different crystal structures, such as mackinawite (FeS_{1-x}), pyrrhotite (Fe₇S₈), cubic ferrous sulfide (FeS), pyrite (FeS₂), troilite (Fe_{1-x}S), or greigite (Fe₃S₄) [16-22].

Despite the many studies of the corrosion process of carbon steel, the corrosion system in the presence of both H₂S and CO₂ is rarely studied. This work aims to elucidate the impact of H₂S content on the H₂S/CO₂ corrosion of pipeline steel under the coexistence of H₂S and CO₂. It is found that this provides insight into the prediction of the potential hazards resulting from corrosion and into the methods for effective control of premature failure.

2. EXPERIMENTS

2.1. Materials

Using electric discharge wire-cutting machining, the laboratory samples were cut into rectangles (25 mm×20 mm×3 mm) from a P110 steel oil casing tube, and their chemical components (wt%) are as follows: C 0.26; Si 0.19; Mn 1.37; P 0.009; S 0.004; Cr 0.148; Ni 0.028; Mo 0.013; Cu 0.019; Nb 0.06; V 0.006; Ti 0.011; and Fe balance. The samples were ground by hand using SiC abrasive paper, ultrasonically cleaned in acetone solution and dried prior to the other treatments.

2.2. Immersion tests

Immersion tests were conducted in an autoclave with a high temperature and pressure under the simulated environment of H₂S/CO₂. The dimensions of the specimens were 14 mm × 10 mm × 4.5

mm. Both at the beginning and end of the tests, the specimens were ultrasonically cleaned with acetone, degreased, washed, dried, and weighed on an analysis balance with the accuracy of 0.1 mg. The experimental solution simulating the development water extracted from one oil field was prepared from analytical reagents and deionized water and included 5 wt% NaCl. This solution underwent 4-hour oxygen deprivation using N₂. These tests were performed for a variety of volumes of a saturated solution of H₂S and CO₂, as well as for a solution free of H₂S or CO₂. The specimens were quickly placed in a uniform temperature water bath, and the starting time of the experiment was set when the bath temperature reached 60°C. 48 hours later, the samples were removed from the water bath. The corrosion rate was calculated using the weight-loss technique.

After the corrosion tests, the specimens were removed from the autoclave, rinsed in deionized water, dehydrated in alcohol and dried in air. One of the four specimens was retained for surface characterization of corrosion scales. The remaining three specimens were descaled in the solution consisting of hydrochloric acid (100 mL, density is 1.19 g/mL), hexamethylene tetramine (5 g), and deionized water (900 mL) at room temperature and then processed as above. Then, the specimens were weighed again to determine the weight loss. The corrosion rate was calculated according to

$$V_{CR} = \frac{8.76 \times 10^4 W}{S \rho t}$$

where V_{CR} is the corrosion rate, mm/y; W is the weight loss, g; S is the exposed surface area of specimen, cm²; ρ is the density of specimen, g/cm³; t is the corrosion time, h; and 8.76×10^4 is the unit conversion constant. The average corrosion rate with error bars was calculated from the three parallel specimens for each test.

2.3. Electrochemical characterization

Using a potentiostat/galvanostat system, the potentiodynamic polarization curves as well as electrochemical impedance spectroscopy (EIS) results of the specimens that were placed in different H₂S concentrations were studied. Prior to the electrochemical measurements, all specimens were wet-ground to 2000 grit using SiC paper and were then polished to a mirror finish, cleaned with acetone ultrasonically, rinsed in distilled water, and dried in warm air. The measurements were carried out in a three-electrode flat cell in which the counter electrode consisted of a Luggin capillary and a large platinum plate. All potential measurements were performed with Ag/AgCl as the reference electrode. It should be emphasized that the EIS test was conducted within the 10⁵-10⁻² Hz frequency range with a sinusoidal potential disturbance of 1 mV. To analyze the EIS data, a fitting simulation of the FRA was adopted. For polarization curve measurements, the scan range of the potential was from -1400 to -100 mV with the scan rate of 1 mV/s. The corrosion potential (E_{corr}) and corrosion current density (i_{corr}) were derived directly from the polarization curves by Tafel region extrapolation.

3. RESULTS AND DISCUSSION

Figure 1A shows the EIS data for the pipeline steel specimens immersed in the carbon dioxide saturated water. Using Nyquist plots, it was found that the diameter of the capacitive loop remained

constant at approximately $120 \text{ k}\Omega \text{ cm}^2$ when the immersion period was less than 5 days. Nevertheless, when the immersion period was increased to 10 days, a rapid decline in the capacitive loop was observed. It could be seen clearly in Figure 1B that the phase angle declined and separated into two peaks when the immersion period rose to 10 days. Table 1 presents the fitting results of the pipeline steel EIS measurements. It was clear that there was a decline in the solution's resistance from $72.5 \text{ k}\Omega/\text{cm}^2$ to $32.6 \text{ k}\Omega/\text{cm}^2$ due to the improved conductivity of the solution when the immersion time increased. The decline of n_f means that the passive film became growingly inhomogeneous or flawed due to the permeation of carbon dioxide. Under the CO_2 corrosion environment, the steel in the matrix showed a strong electron affinity to OH^- [23].

Table 1. Fitting results of the pipeline steel EIS measurements in carbon dioxide saturated water for a variety of immersion periods.

| Immersion time | $R_s (\Omega\text{cm}^2)$ | $R_f (\Omega\text{cm}^2)$ | $R_{ct} (\Omega\text{cm}^2)$ |
|----------------|---------------------------|---------------------------|------------------------------|
| 0 Day | 72.5 | 133.5 | 91.0 |
| 5 Days | 70.6 | 121.6 | 84.6 |
| 10 Days | 57.7 | 63.5 | 49.2 |
| 20 Days | 32.6 | 1.11 | 3.25 |

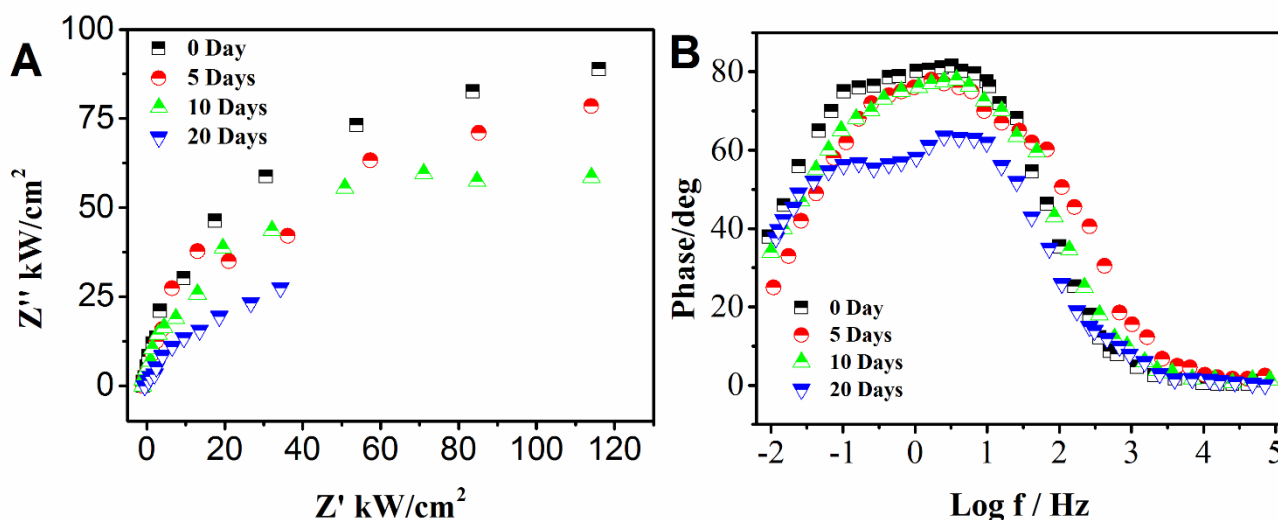


Figure 1. Changes of the Nyquist plots (A) as well as plots of the phase angle (B) of the pipeline steel in carbon dioxide saturated water for a variety of immersion periods.

Table 2. Average corrosion rate of steel placed in different H_2S concentrations under the coexistence of H_2S and CO_2 ($C_{\text{CO}_2} = 10 \text{ mM}$).

| | | | | | | | |
|--------------------------------------|-------|-------|-------|-------|-------|-------|-------|
| $\text{P}_{\text{H}_2\text{s}}$ (mM) | 0 | 0.05 | 0.1 | 0.2 | 0.8 | 2 | 4 |
| V_{CR} (mm/a) | 0.347 | 0.325 | 0.259 | 0.262 | 0.254 | 0.263 | 0.267 |

Table 2 presents the data for the corrosion rates of the steel placed in different H₂S concentrations under the environment where H₂S coexists with CO₂ (C_{CO2} = 10 mM). It was found that the general corrosion rate of the steel under the environment containing CO₂ only was 0.347 mm/a. Nevertheless, with the addition of a small quantity of H₂S, the corrosion rate was reduced to 0.25 mm/a. When the H₂S content was raised to 2 mM from 0.05 mM, no evident variation was observed in the corrosion rate. With the increase of the H₂S concentration, the corrosion rate tended to improve. In other words, the addition of a small amount of H₂S has an inhibitive effect on CO₂ corrosion. Generally, the corrosion rate increases with increasing H₂S concentration [24]. In the case of a sufficiently high H₂S concentration, the situation may be different. The decrease of the corrosion rate with the increase H₂S concentration was also observed by other researchers [25, 26].

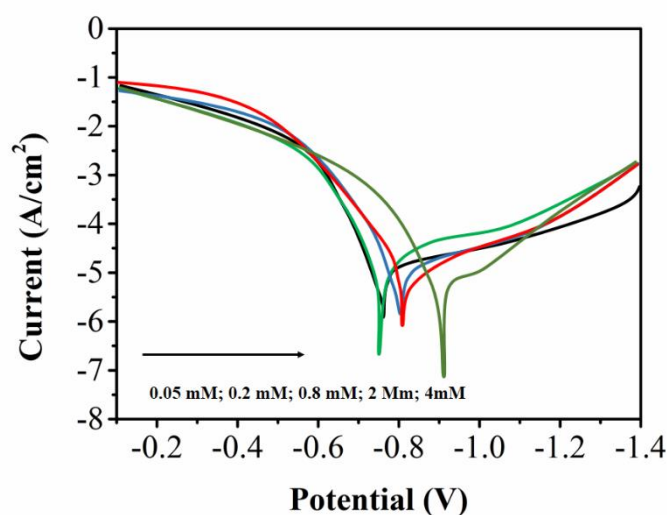


Figure 2. Potentiodynamic polarization curves of the steel placed in different H₂S concentrations under the coexistence of H₂S and CO₂ (C_{CO2} = 10 mM).

The potentiodynamic polarization curves of the steel placed in different H₂S concentrations under the coexistence of H₂S and CO₂ (C_{CO2} = 10 mM) are shown in Figure 2. Table 3 presents the corrosion parameters deduced from the potentiodynamic polarization curves. As the concentration of H₂S decreased from 0 to 0.2 mM, a moderate negative switching in the steel corrosion potential (E_{corr}) was observed, while with the increase of the H₂S concentration, the corrosion current density (i_{corr}) declines accordingly. All of these results demonstrate that the corrosion of pipeline steel is restrained under the environment of low H₂S concentration. Due to the existence of H⁺, cathodic polarization is relieved, facilitating the electrons flowing to cathode so that the corrosion process is enhanced; this is known as the hydrogen depolarization corrosion [27]. When the H₂S concentration is increased from 0.8 mM to 4 mM, the i_{corr} rises step by step, demonstrating that the growing concentration of H₂S concentration can accelerate steel corrosion. These outcomes are in accordance with data relevant to the corrosion rate. An increase in the corrosion current density of the specimen of steel was observed when the H₂S concentration was increased. For the vacant substrate on the steel, it can be seen in Table 3 that compared to the low H₂S concentration environment, the high H₂S

concentration environment corrosion's potential E_{corr} revealed a positive displacement from -720 mV to -911 V. This results from the decomposition effects on the substrate contributed by H_2S .

Table 3. Electrochemical polarization parameters for the steel with coexistence of H_2S and CO_2

| Sample | E_{corr} (mV) | I_{corr} (mA/cm ²) | b_a (mV/dec) | b_c (mV/dec) |
|--------|---------------------------|--|----------------|----------------|
| 0.05 | -720 | 4.22 | 87 | 114 |
| 0.2 | -731 | 4.47 | 59 | 89 |
| 0.8 | -797 | 4.58 | 79 | 95 |
| 2 | -806 | 4.60 | 72 | 94 |
| 4 | -911 | 4.72 | 81 | 90 |

It has been shown that EIS is a useful technique for the characterization of the surface layers as well as for the investigations of the $\text{H}_2\text{S}/\text{CO}_2$ corrosion systems[18]. Figure 5 shows the EIS Nyquist plot of the steel placed in different H_2S concentrations under the coexistence of H_2S and CO_2 ($C_{\text{CO}_2} = 10$ mM). When the H_2S concentration is in the 0–0.2 mM range, great capacity reactance arcs are developed at high frequencies, while inductance reactance arcs are developed at low frequencies. In $\text{H}_2\text{S}/\text{CO}_2$ corrosion environments, CO_2 and H_2S are hydrolyzed to form H^+ . Hydrogen atoms [H] generated from the cathodic process of the electrochemical reaction desorbed mainly in two forms from the electrode surface. The commonly acceptable mechanism is that the process of hydrogen atoms generated from the reduction reaction bonding to each other as molecules is impeded because of the strong absorbability of H_2S , HS^- and S^{2-} on the electrode surface; on the other hand, the process of hydrogen atoms diffusing into the metal matrix is enhanced strongly, so that hydrogen atoms may gather at crystal defect points such as inclusions and grain boundaries, or exist in the crystal lattice in the form of an interstitial atom; and both of these mechanisms lead to a degradation in the mechanical properties of the metal material and to a remarkable increase in susceptibility. The reactance arcs developed at high frequencies are related to both the dual-layer capacitance and the transfer resistance, whereas the reaction arcs developed at low frequencies are likely to be related to the adsorption and isolation of the intermediate products appearing on the electrode surface, namely, FeHS^+ under the $\text{H}_2\text{S}/\text{CO}_2$ environment ($C^{\text{CO}_2} = 10$ mM) [28], in which FeHS^- ions are adsorbed upon the appearance of the corrosion product film. The intermediate products FeHS^+ can generate FeS_{1-x} or Fe^{2+} directly through hydrolysis. In addition, Fe^{2+} can generate FeS or $\text{Fe}(\text{HS})_2$ by reacting with HS^- or H_2S [29, 30].

The semi-diameter of capacity reactance arcs developed at high frequencies reveal an evident rise with increasing H_2S concentration when the concentration is lower than 0.2 mM, indicating the charge relaxation course of the electric dual layer. Not only is the time constant but also the charge transfer resistance is improved. Features of inductance reactance arcs developed at low frequencies tend to become more obvious. When a small quantity of H_2S is added, the anode reaction area declines, resulting from continuous adsorption and disconnection of more FeS deposition or more

FeHS^+ ions on the steel surface. At the same time, the double-layer capacitance decreases with the rise of adsorptive power of anions, indicating that the corrosion course is restrained.

When the H_2S concentration is within the 0.8–4 mM range, the semi-diameter of the capacity reactance arcs developed at high frequencies clearly declines with the rise of the H_2S concentration, accelerating the electric double layer's charge relaxation course. Declines in both the time constant and the charge transfer resistance are observed. This indicates that the increased H_2S concentration can act as a promoter of the corrosion process. An arc that is similar to a capacity reactance arc can be seen in the low-frequency area, which likely to be due to the disintegration of the sulfide film. Consequently, for the sulfide film developed on the electrode surface with many flaws, its discontinuities and drawbacks rise with the improvement of H_2S concentration, further promoting the corrosion process.

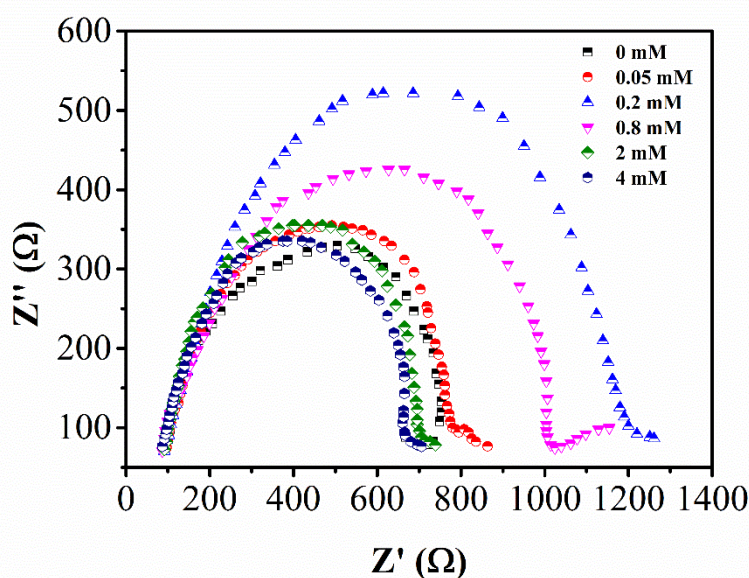


Figure 5. EIS Nyquist plot of steel placed in different H_2S concentrations under the coexistence of H_2S and CO_2 ($C_{\text{CO}_2} = 10$ mM).

There is a difference between the equivalent circuit applied for the purpose of fitting the EIS results for the steel for the H_2S concentration within the 0–0.2 mM range, and the equivalent circuit applied for the purpose of fitting EIS results for the steel when the H_2S concentration is in the 0.8–4 mM range. The equivalent circuits' parameters are defined as follows: R_s represents the electrolyte resistance between the working electrode and the control electrolyte; Q_{dl} represents the fixed phase element of the electric double layer capacity between the electrolyte and the corrosion product film; R_t represents the charge transfer resistance; L represents the inductive resistance; RL represents the inductive reactance resistance; C represents the fixed phase element of the corrosion product film capacitor, and RC represents the film resistance. The R_t values of the steel placed in different H_2S concentrations under the coexistence of H_2S and CO_2 ($C_{\text{CO}_2} = 10$ mM) are shown in Figure 6 and were fit using the ZSIMPWIN program package. The R_t rises quickly when the H_2S concentration increases to 0.2 mM from 0 mM. By contrast, the R_t declines slightly when the concentration range of H_2S is 0.8

mM to 4 mM. The R_t relies greatly on the corrosion product film on the steel surface. With the micro-concentration of H_2S , the density of the film structure tends to be higher with the growing H_2S concentration and the overlapping and the adhesion stress of the corrosion product film are enhanced continuously, leading to a higher resistance for the charge through the electric double layer; therefore, the corrosion course is restrained. When the H_2S concentration grows further, some sections of the corrosion product film become less dense and even decrease, and the protective effect of the corrosion product film is deteriorated. The R_t declines step by step, showing that the corrosion behavior occurs faster. These results are in accordance with data in connection with the corrosion rate.

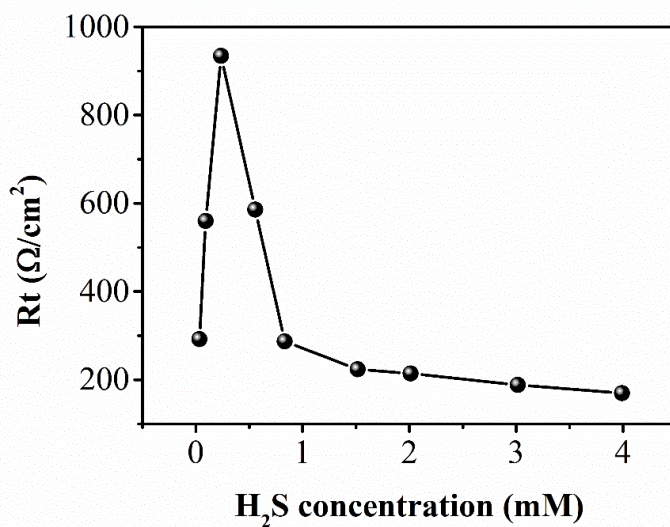


Figure 6. Charge transfer resistance of the steel placed in different H_2S concentrations under the coexistence of H_2S and CO_2 ($C_{CO_2} = 10$ mM).

4. CONCLUSIONS

Under an environment where H_2S coexists with CO_2 ($C_{CO_2} = 10$ mM), a decline in the general corrosion rate is observed with the rise in H_2S concentration, and later, the rate shows an improvement tendency. With further improvement of H_2S concentration, the steel tends to exhibit localized corrosion. Under the environment where H_2S coexists with CO_2 ($C_{CO_2} = 10$ mM) and the concentration of H_2S is within the scope of 0–0.2 mM, more FeS deposition is generated or more $FeHS^+$ ions adsorb and disintegrate continuously on the electrode surface with the rise of H_2S concentration; as a result, the inhibition of the corrosion process is accomplished. Under the environment where H_2S coexists with CO_2 ($C_{CO_2} = 10$ mM) and the concentration range of H_2S is within 0.8–4 mM, some sections of the corrosion product film tend to be less dense and even removed, and the protective effect of the corrosion product film is deteriorated; as a result, the corrosion process is accelerated.

References

1. D. Shoesmith, P. Taylor, M. Bailey and D. Owen, *Journal of the Electrochemical Society*, 127

- (1980) 1007.
2. D. Shoesmith, T. Rummery, M. Bailey and D. Owen, *Journal of the Electrochemical Society*, 127 (1980) 27.
 3. T. Kudo, H. Tsuge and T. Moroishi, *Corrosion*, 45 (1989) 831.
 4. S. Al-Hassan, B. Mishra, D. Olson and M. Salama, *Corrosion*, 54 (1998) 480.
 5. J. Al-Hajji and M. Reda, *Corrosion*, 49 (1993) 363.
 6. Y. Zheng, J. Ning, B. Brown and S. Nešić, *Corrosion*, 72 (2016) 679.
 7. G. Schmitt, *Corrosion*, 47 (1991) 285.
 8. J. Crolet, *Matériaux & Techniques*, 104 (2016) 206.
 9. K. Videm and J. Kvarekvål, *Corrosion*, 51 (1995) 260.
 10. O. Conlette, N. Emmanuel and O. Chijoke, *Microbial Ecology*, 72 (2016) 175.
 11. A. Ikeda, S. Mukai and M. Ueda, *Corrosion*, 41 (1985) 185.
 12. D. Jingen, Y. Wei, L. Xiaorong and D. Xiaoqin, *Petroleum Science and Technology*, 29 (2011) 1387.
 13. S. Collins, K. Davey, J. Chu and B. O'Neill, *Chemeca 2016: Chemical Engineering-Regeneration, Recovery and Reinvention*, (2016) 209.
 14. H. Ma, X. Cheng, G. Li, S. Chen, Z. Quan, S. Zhao and L. Niu, *Corrosion science*, 42 (2000) 1669.
 15. E. Abelev, T. Ramanarayanan and S. Bernasek, *Journal of The Electrochemical Society*, 156 (2009) C331.
 16. S. Nešić, *Corrosion Science*, 49 (2007) 4308.
 17. Z. Yin, W. Zhao, Z. Bai, Y. Feng and W. Zhou, *Electrochimica Acta*, 53 (2008) 3690.
 18. A. Davoodi, M. Pakshir, M. Babaiee and G.R. Ebrahimi, *Corrosion Science*, 53 (2011) 399.
 19. J. Tang, Y. Shao, J. Guo, T. Zhang, G. Meng and F. Wang, *Corrosion Science*, 52 (2010) 2050.
 20. Y. Qi, J. Yang, C. Zhang and Z. Zhang, *Corrosion Engineering, Science and Technology*, 51 (2016) 507.
 21. C. Man, C. Dong, H. Xue, K. Xiao, X. Li and H. Qi, *International Journal of Minerals, Metallurgy, and Materials*, 23 (2016) 769.
 22. Z. Wang and J. Zhang, *Corrosion Reviews*, 34 (2016) 17.
 23. X. Huang, Y. Qi, C. Chen, H. Yu and G. Lu, *Corrosion Engineering Science & Technology*, 50 (2015) 169.
 24. R. Elgaddafi, R. Ahmed and S. Shah, *Research Journal of Applied Sciences Engineering & Technology*, 13 (2016) 510.
 25. L. Zhang, R. Ding, J.W. Yang and M. Lu, *Journal of University of Science & Technology Beijing*, 31 (2009) 563.
 26. Z. Yin, W. Zhao, Z.Q. Bai, Y. Feng and W. Zhou, *Electrochimica Acta*, 53 (2008) 3690.
 27. C. Wang, *Materials Science Forum*, 852 (2016) 90.
 28. L. Xu and Y. Cheng, *Corrosion Science*, 51 (2009) 2330.
 29. D. Rickard, *Chemical Geology*, 78 (1989) 315.
 30. D. Rickard, *Geochimica et Cosmochimica Acta*, 59 (1995) 4367.